Lasing in topological edge states of a one-dimensional lattice

P. St-Jean[1]*, V. Goblot[1], E. Galopin[1], A. Lemaître ⓘ[1], T. Ozawa[2], L. Le Gratiet[1], I. Sagnes[1], J. Bloch[1] and A. Amo[1]

[1]Centre de Nanosciences et de Nanotechnologies, CNRS, Université Paris-Sud, Université Paris-Saclay, C2N - Marcoussis, 91460 Marcoussis, France.
[2]INO-CNR BEC Center and Dipartimento di Fisica, Università di Trento, I-38123 Povo, Italy. *e-mail: philippe.st-jean@c2n.upsaclay.fr

Supplementary information: Lasing in topological edge states of a 1D lattice

I. CHIRAL SYMMETRY OF THE SSH HAMILTONIAN

A system exhibits chiral symmetry if there exists a unitary transformation $\mathcal{U}_c$ that anticommutes with the Hamiltonian[1]: $\{H,\mathcal{U}_c\} = 0$. For an infinite SSH lattice, the Hamiltonian of the system (defined in Eq. 1 of the main text) can be expressed in momentum space by a 2×2 matrix

$$H(k) = \vec{d}(k) \cdot \vec{\sigma}, \tag{1}$$

where $\sigma_{x,y,z}$ are the Pauli matrices, and

$$\begin{aligned}
d_x(k) &= t + t' cos(ka) \\
d_y(k) &= t' sin(ka) \\
d_z(k) &= 0,
\end{aligned} \tag{2}$$

with a the unit cell dimension[2].

The SSH Hamiltonian thus possesses a chiral symmetry defined by the Pauli matrix σ_z: $\{H(k), \sigma_z\} = 0$. The principal consequence of this symmetry is that the energy spectrum is symmetric around the origin: every eigenstate $|u_E\rangle$ with eigenenergy E has a partner $|u_{-E}\rangle = \sigma_z |u_E\rangle$ with energy $-E$. For states with energy $E = 0$ (such as the topological edge states considered in this work), these states are their own partner ($E = -E = 0$), and their spectral position is not affected by perturbations, as long as $\{H(k), \sigma_z\} = 0$.
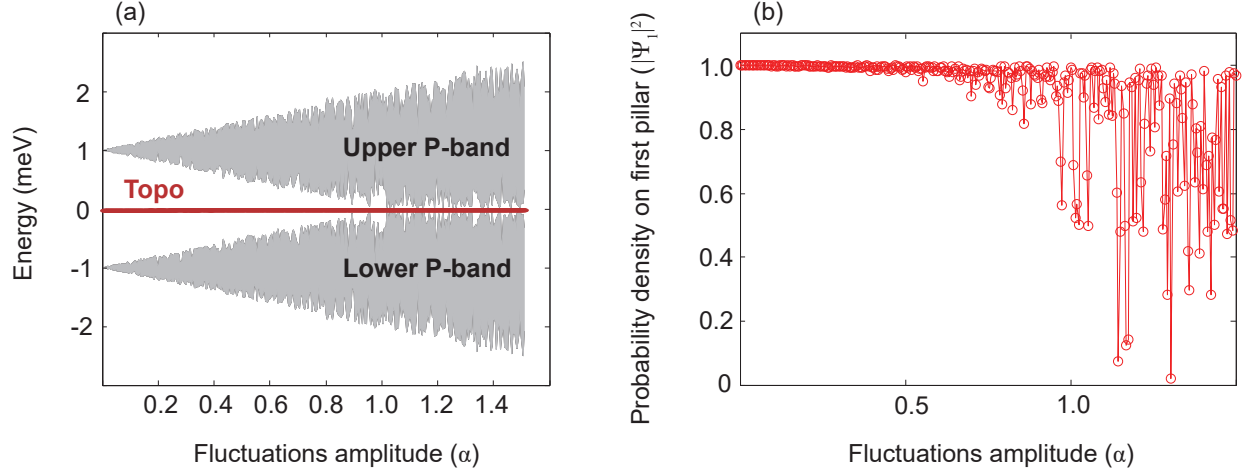

FIG. S1. Evolution of the energy (a) and probability density on first pillar (b) of the p_y topological edge state as a function of the amplitude of the hopping fluctuations. Gray areas in panel (a) indicate the width of the P-bands.

For example, perturbations that affect the hopping strengths t and t' only modify off-diagonal terms in Hamiltonian 1 and thus do not affect chiral symmetry. Consequently, the spectral positions of zero-energy states (such as the topological edge states of the p_y sub-space discussed in this work) are immune to such perturbations. This can be seen by diagonalizing a Hamiltonian similar to that used for calculating the band structure presented in Fig. 1 (e) of the main text, but where we include random fluctuations to the hopping strengths: $t_{l,t}^{(i)} \rightarrow t_{l,t}^{(i)}(1 + \alpha r_{l,t}^{(i)})$, where $r_{l,t}^{(i)}$ are random numbers between -1 and 1, α describes the amplitude of the hopping fluctuations, and i refers to the site number along the chain.

Fig. S1 (a) indeed shows that the spectral positions of the p_y topological edge state (red line) is not affected by fluctuating hopping strengths. However, the width of the upper and lower P-bands, indicated by grey areas, increases constantly following a stochastic evolution. This increase is due to the statistical loss of contrast between t_t and t_l. According to Fig. S1 (b) however, the localization of the edge does not significantly change under such perturbations, as long as the magnitude of the perturbation is lower than the hopping energies ($\alpha > 1$).

Thus, perturbing hopping strengths does not provide the most compelling platform for investigating the robustness of the topological edge modes, because chiral symmetry of the SSH Hamiltonian insures that their energy will not be affected. On the other hand, perturbations that break chiral symmetry by adding diagonal terms to the Hamiltonian, such as considering second-neighbour hopping or different on-site energies, have more drastic consequences as they modify the spectral position of the topological edge state. This is the case in our work, where we locally break chiral symmetry by modifying the on-site energy of the edge pillar. The consequences of this perturbation are presented in the section *Robustness of topological lasing* of the main text.

Furthermore, another perturbation of the lattice that could be investigated corresponds to fluctuations of the angle between successive links of the zigzag chains. Deviations from 90° would cause mixing of the p_x and p_y orbitals, and, thus, of the trivial and non-trivial sub-spaces. However, this effect is not a feature of the general SSH Hamiltonian presented in Eq. (1) of the main text, as it requires the topologically trivial and non-trivial sub-spaces to be simultaneously supported by the structure. Therefore, we have not investigated in further details its impact when determining the robustness of topological lasing. Note that the very high resolution of the electron beam lithography employed to fabricate our samples (below 20 nm) allows discarding such angle fluctuations.

II. TIGHT-BINDING CALCULATIONS OF THE ORBITAL WAVE-FUNCTIONS

Eigenstates of the $p_{x,y}$ sub-spaces can be theoretically calculated by diagonalizing the Hamiltonian presented in Eq. 1 of the main text. In the case at hand, t and t' are replaced by $t_l = 1$ meV and $t_t = 0.15$ meV for the p_x sub-space, and vice-versa for the p_y sub-space (these values are extracted from the direct measurement of the amplitude and energy gap of the P-bands). For a chain formed from $N = 20$ micropillars, each sub-space is formed from 20 eigenstates distributed in two conduction bands separated by a band gap of 1.7 meV (see Fig. 1 (b) and (e) of the main text).
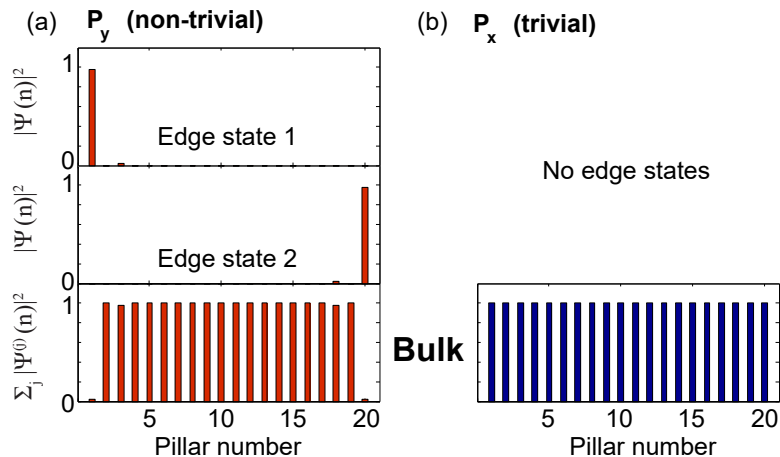

FIG. S2. (a) Top and middle panels: distribution over every pillar of the wave-function squared amplitude of both gap states. Bottom panel: summation of the wave-function squared amplitudes of all 18 bulk states of the p_x sub-space. (b) Similar for the p_y sub-space, where there are no edge states.

As presented extensively in the main paper, two gap states in the p_y sub-space are localized at each end of the chain as a consequence of the non-trivial topology associated to the dimerization $t' > t$. The localization of these gap states can be visualized by considering the distribution of their wave-function over every site of the chain, as presented in the top and middle panels of Fig. S2 (a). The strong hopping anisotropy of p-orbitals leads to a strong localization of the edge state on the first pillar, with $|\psi_1|^2 > 0.95$. Therefore, even lattices formed from a few unit cells would show independent localized states on each edge.

Another important consequence of the non-trivial topology is that the wave-functions of the 18 bulk states (i.e. states with energies in the conduction bands) strongly vanishes at the edge pillars. This is clearly seen by summing

the wave-functions squared amplitude of the 18 bulk states. The distribution of this summation over every pillar of the chain is presented in the bottom panel of Fig. S2 (a), and clearly shows a vanishing value at the position of the edge pillars. Interestingly, introducing in the middle of the chain a defect that interchanges the inter- and intra-cell hopping energies (e.g. by removing one pillar, see Ref. 3) would lead to the emergence of similar topological states in the middle of the lattice.

For the p_x sub-space, the edge pillars are strongly coupled to the rest of the chain resulting in the topologically trivial phase of the SSH model. Therefore, there are no gap states in this sub-space, and the 20 eigenstates are delocalised over every pillar including the edge pillars (see Fig. S2 (b)).

III. EMISSION SPECTRA OF THE LASER

In Section *Lasing in the topological edge state* of the main text, we provide spectrally resolved images of the PL that are clearly dominated, in the lasing regime, by emission from the topological mode. In Fig. S3, we supply emission spectra measured at the edge of the chain (corresponding to slices at x = 0 μm for images similar to those presented in Fig. 3 (c) and (d) of the main text) for excitation below (a), at (b), and above (c) the lasing threshold. The spectra are limited to energies around the P-bands.

Above the lasing threshold, the linewidth of the emission becomes narrower (from 74 vμeV down to 31 μeV – limited by our detection resolution) as reported in Fig. 3 (b) of the main text. Above threshold, the nonlinear increase of the emission from the topological mode (labelled Topo) overcomes that from the bulk bands. A blueshift of the emission is observed due to the interaction with the exciton reservoir.
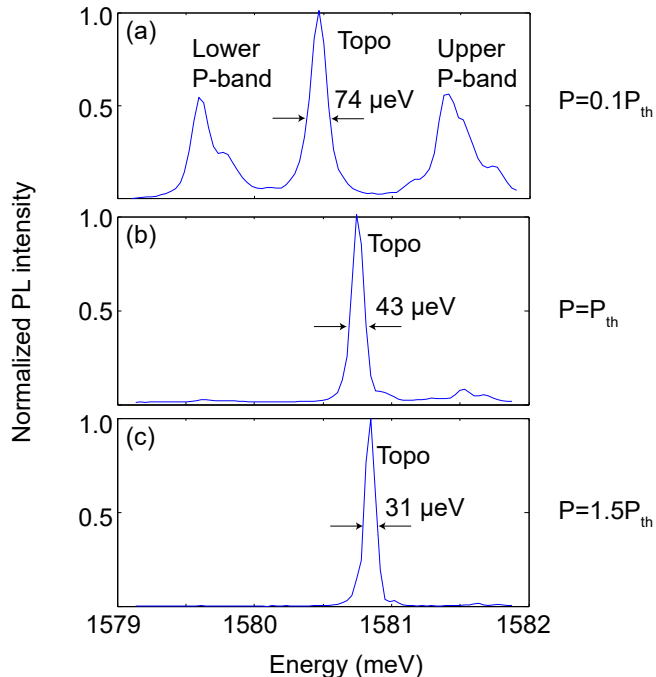

FIG. S3. Emission spectra taken at x=0 according to PL images in Fig. 3 (c)-(d) of the main text for excitation below (a), at (b), and above (c) the lasing threshold.

IV. POLARITON LASING USING A LOCALIZED EXCITATION

Under a localized excitation (the situation shown in Fig. 4 of the main text), the lasing threshold is reduced by an order of magnitude with respect to the case of an extended excitation spot (Fig. 3 of the main text), down to $P_{th} = 3.1$ mW. Above this threshold, a non-linear increase of the emission is observed in the I-P curve presented in Fig. S4 (b). PL images as a function of position and emission energy still show that, in the lasing regime, emission from the topological edge state completely overcomes that from bulk bands (see Fig. S4 (d)-(e)). As well, the topological

edge state is almost completely localized over the last pillar as depicted in the inset, even at the strongest excitation power used ($P_{ex} = 6P_{th} = 18$ mW). The smaller area covered by the pump allows to reach higher power densities (up to 190 W/cm^2) than with the extended spot. At the highest power densities investigated, we see no indication of degradation of the device performance.

Similarly as with the large excitation spot, polariton lasing leads to a narrowing of the emission linewidth which, above the lasing threshold, becomes limited by the spectral resolution of the detection setup. On the other hand, interactions with the localized reservoir are more important, leading to a stronger spectral blueshift (both effects are respectively presented by the blue circles and black squares in Fig. S4 (c)).

For the large excitation spot, we observed a rigid shift of all the band structure: of bulk bands as well as of the edge state. Under a localized excitation spot, the chiral symmetry is broken as described in the previous section, and the induced blueshift of the last pillar only changes the spectral position of the edge state. Thus the topological mode sweeps across the energy gap as the excitation power is increased, as shown in Fig. S4 (d) and (e)).

It is interesting to notice that the density of excitation power at the lasing threshold is similar to that measured with the extended excitation spot as both the threshold power and spot size are reduced by an order of magnitude. This indicates that P_{th} is not very sensitive to the on-site energy perturbations in the first pillar, a direct consequence of the robust localization of the topological edge state.
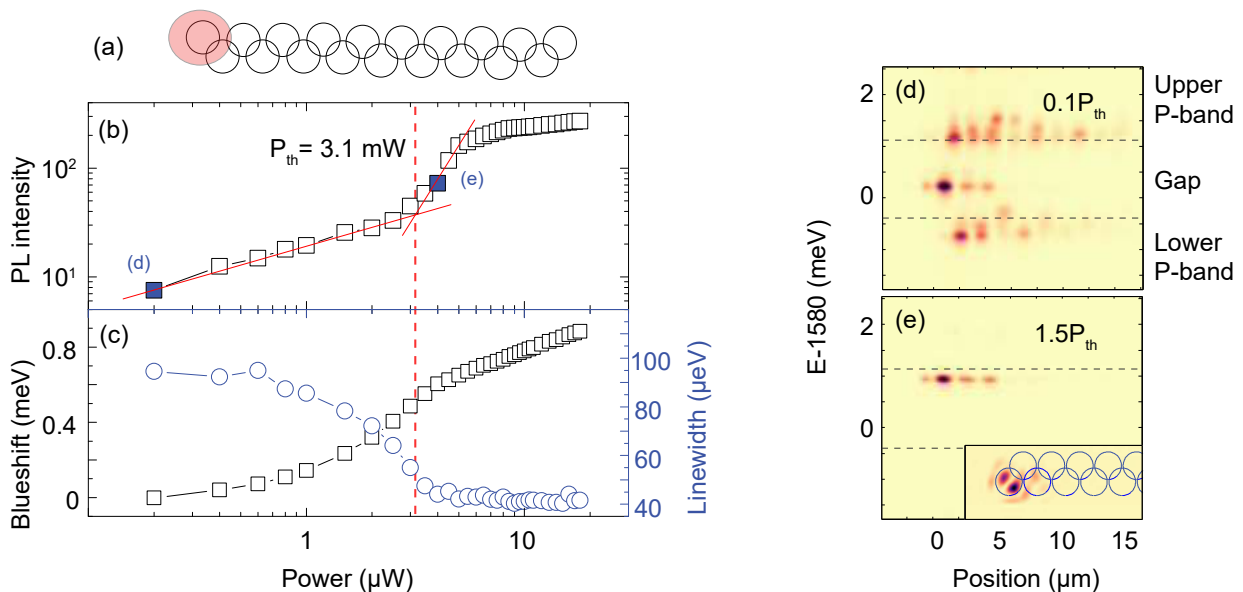
FIG. S4. (a) Schematic representation of the localized excitation scheme. (b) Integrated PL intensity as a function of the excitation power. The red dashed line indicates the position of the lasing threshold. (c) Measured PL linewidth (blue circles) and spectral blueshift (black squares) of the topological edge state as a function of the excitation power. (d)-(e) PL intensity as a function of emission energy and position along the chain for an excitation power below (d) and above (e) the lasing threshold; the excitation power for each measurement is indicated by the blue squares in Panel (b). Inset in Panel (e) shows a spatial image of the PL at the energy of the topological edge state.

V.   TAMM STATES IN THE TOPOLOGICALLY TRIVIAL p_x SUB-SPACE

The local perturbation created by the localized excitation used in the section "Robustness of the topological lasing" of the main text leads to the appearance of localized states in the topologically trivial p_x sub-space. Hereafter, we present theoretical tight-binding calculations (considering a chain of 20 pillars) describing the appearance of these states as a function of the energy associated to the local perturbation U_1.

The top line of Fig. S5 shows the evolution of the p_x band structure for perturbations energies of $U_1 = 0$ meV (a), 0.2 meV (b), 0.4 meV (c), 0.6 meV(d), and 0.8 meV (e). In each figure, the position of Tamm states (or the

corresponding bulk states for $U_1 = 0$ meV in (a)) is indicated by blue circles. The middle and bottom lines present the distribution of the wave-functions over every pillar for Tamm$_1$ and Tamm$_2$, respectively. We see that for $U_1 \to 0$, these states are completely delocalised over the whole lattice. Then, as the perturbation energy increases, the wave-functions become more localized, and, at highest energies, they are strongly localized on the first two pillars of the chain. These evolutions of the energy and localization of the Tamm states are presented in more details in Fig. 4 (c) and by the blue curves in Fig. 4 (f) of the main text, respectively.

This situation is drastically different for the topologically non-trivial edge state in the p_y sub-space. There, as shows the red curve in Fig. 4 (f) of the main text, the localization is very strong in the unperturbed chain, and does not change significantly with the perturbation energy as long as its energy stays below that of the upper p-band.
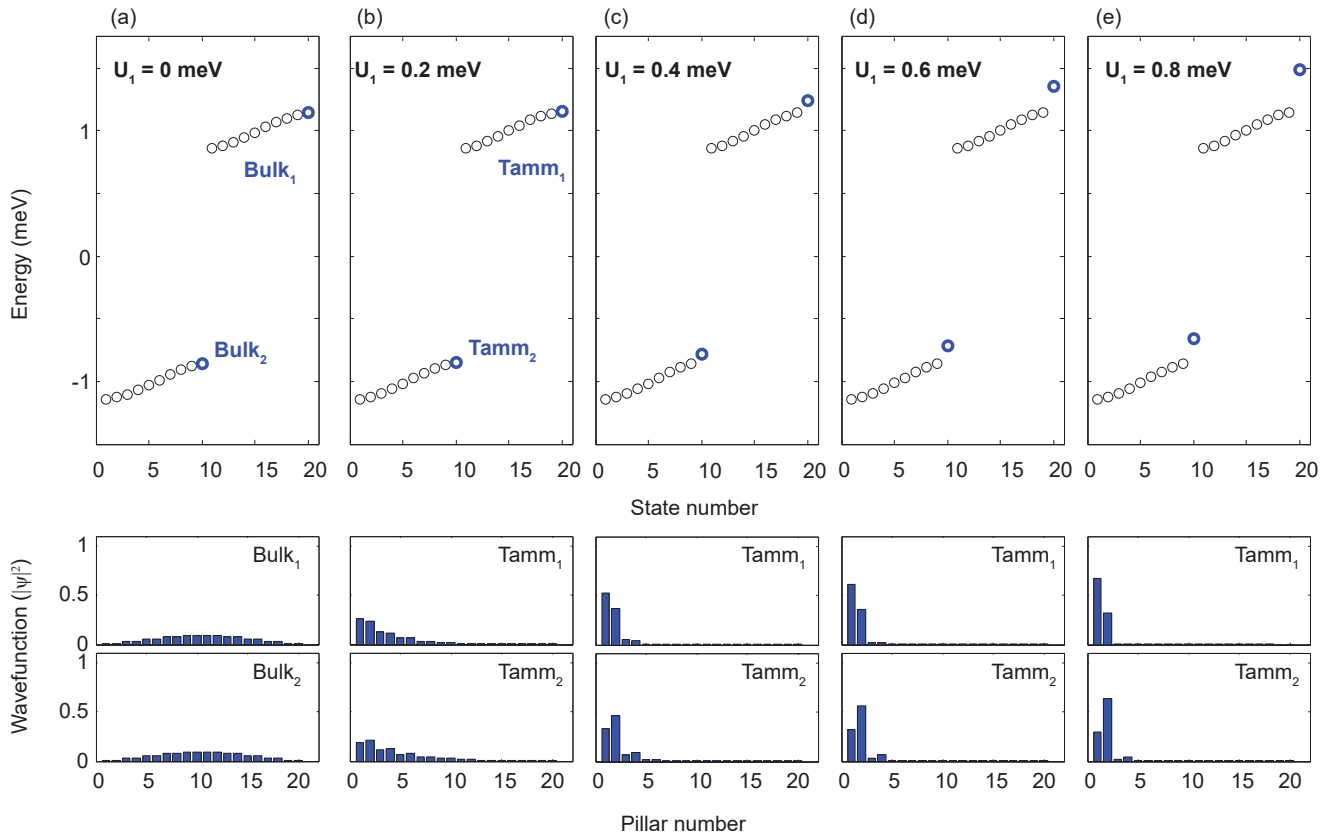

FIG. S5. *Top line.* Evolution of the band structures associated to the topologically trivial p_x sub-space for different values of the perturbation energy U_1 (a)-(e). The position of Tamm states Tamm$_{1,2}$ are indicated by blue circles. *Middle line.* Distribution of the wave-function of Tamm$_1$ over the pillars of a chain formed from 20 pillars for different values of the perturbation energy U_1. *Bottom line.* Distribution of the wave-function of Tamm$_2$ over the pillars of a chain formed from 20 pillars for different values of the perturbation energy U_1.

VI. EXPERIMENTAL SETUP

A schematic diagram of the experimental setup is presented in Fig. S6. The cryostat holds the sample at a temperature of T = 4 K. The PL is detected by a set of lenses L$_{1,2,3}$, a spectrometer and a CCD camera. Imaging of the momentum and real spaces is realized by changing the set of lenses to the configurations presented in Fig. S7 (a) and (b), respectively.
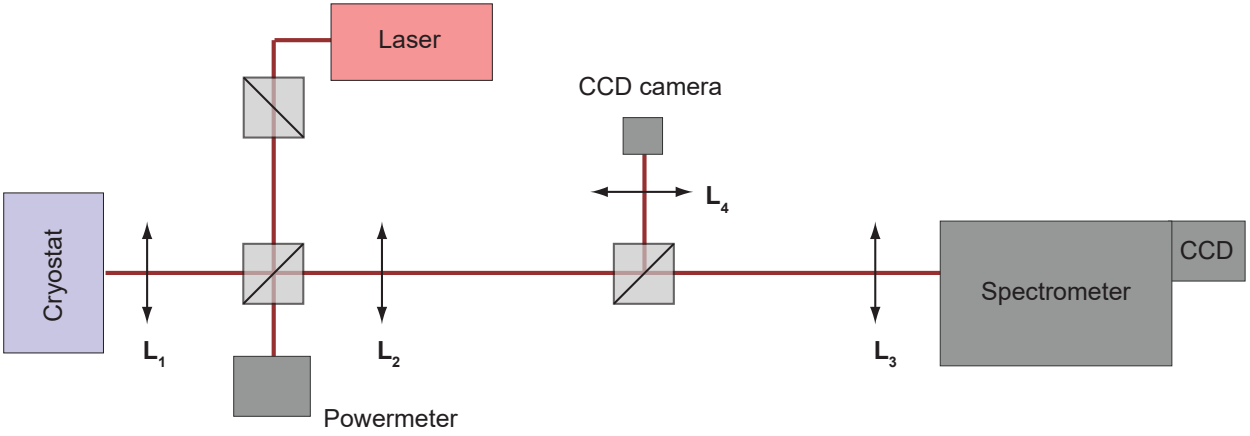
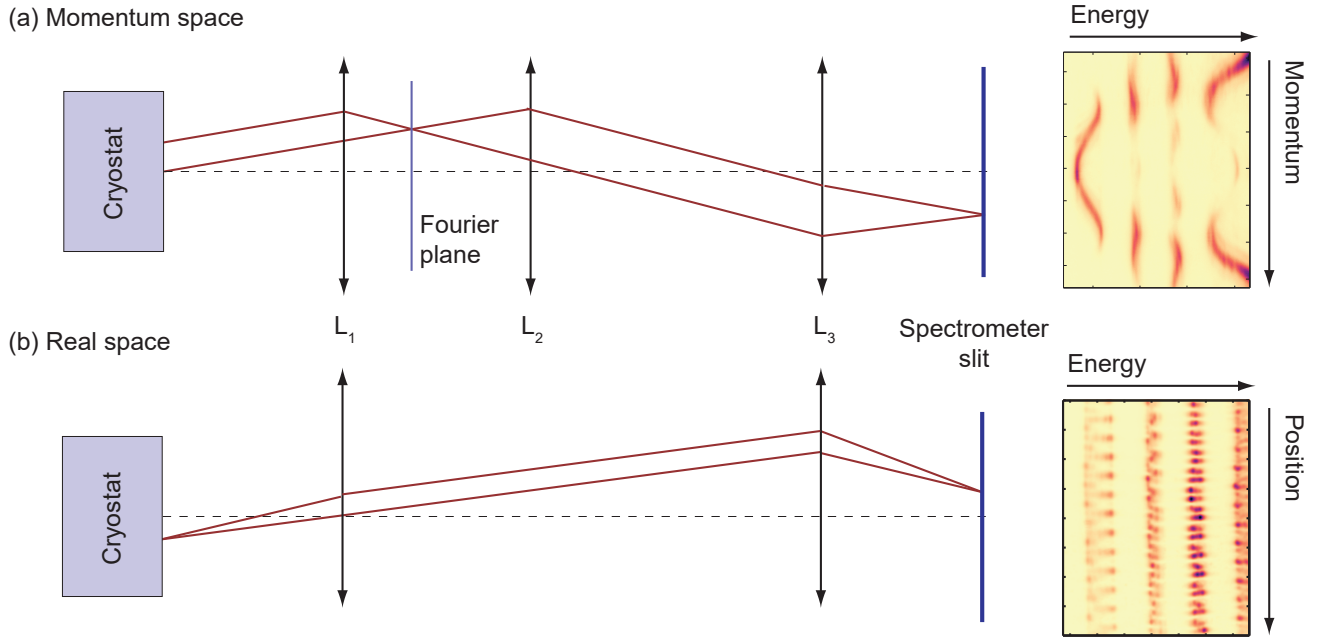FIG. S6. Schematic diagram of the experimental setup.

FIG. S7. Configuration of lenses $L_{1,2,3}$ for imaging the real (a) and momentum (b) spaces.

[1] Chiu, C.-K., Teo, J. C., Schnyder, A. P. & Ryu, S. Classification of topological quantum matter with symmetries. *Reviews of Modern Physics* **88**, 035005 (2016).

[2] Delplace, P., Ullmo, D. & Montambaux, G. Zak phase and the existence of edge states in graphene. *Physical Review B* **84**, 195452 (2011).

[3] Solnyshkov, D., Nalitov, A. & Malpuech, G. Kibble-Zurek Mechanism in Topologically Nontrivial Zigzag Chains of Polariton Micropillars. *Physical Review Letters* **116**, 046402 (2016).